Domain structure of epitaxial $SrRuO_3$ thin films

G. Herranz, F. Sánchez, and J. Fontcuberta
Institut de Ciència de Materials de Barcelona, CSIC, Campus UAB, Bellaterra 08193 (Barcelona), Spain

M. V. García-Cuenca, C. Ferrater, and M. Varela
Departament de Física Aplicada i Òptica, Universitat de Barcelona, Diagonal 647, Barcelona 08028, Spain

T. Angelova, A. Cros, and A. Cantarero
Institut de Ciència de Materials, Universitat de València, P.O. Box 22085, E-46071 València, Spain
(Received 23 September 2004; revised manuscript received 23 December 2004; published 17 May 2005)

Growth of multidomains in epitaxial thin-film oxides is known to have a detrimental effect on some functional properties, and, thus, efforts are done to suppress them. It is commonly accepted that optimal properties of the metallic and ferromagnetic $SrRuO_3$ (SRO) epitaxies can only be obtained if vicinal $SrTiO_3$ (001) (STO) substrates are used. It is believed that this results from the suppression of multidomain structure in the SRO film. Here we revise this important issue. Nanometric films of SRO have been grown on STO(001) vicinal substrates with miscut (θ_V) angles in the $\sim 0.04°$–$4°$ range. Extensive structural analysis by x-ray-reciprocal space maps and μ-Raman spectroscopy indicates that single-domain, orthorhombic, SRO films are already obtained on the almost singular ($\theta_V \approx 0.1°$) substrate, and, thus, substrates with large miscut angles are not required to grow twin-free films. In spite of this, transport properties are found to be optimized for films grown on vicinal substrates ($\theta_V \geqslant 2°$). We claim that this is the result of the change of the growth mode and the resulting film morphology rather than the change of the domain structure. These findings drive the attention to the relevance of the growth mechanism at the initial stages of film growth, and we discuss its implications in other areas of oxide epitaxies. Moreover, we show that in clamped epitaxies on cubic substrates, in spite of isotropic biaxial substrate-induced strains, films may have an in-plane orthorhombic symmetry which results from the internal degree of freedom defined by rotations of the oxygen octahedrons.

DOI: 10.1103/PhysRevB.71.174411 PACS number(s): 61.72.Mm, 78.30.−j, 68.55.Jk, 73.50.−h

I. INTRODUCTION

Epitaxies of oxide materials, such as high-T_C superconductors, ferroelectrics, or colossal magnetoresistive compounds, are getting a prominent role in research and applications. Many of these applications require a detailed control of the epitaxies, and single-crystalline films are required. However, quite commonly, twinning occurs and some relevant functional properties (critical current, magnetic anisotropy, electric polarization) are severely affected.

$SrRuO_3$ (SRO) is attracting a lot of attention because of its metallic properties (its room-temperature resistivity is of about 200 $\mu\Omega$ cm), and it is being employed as an electrode in several oxide-based devices.[1] It is remarkably resistant to corrosion, and this strong chemical stability makes its use very appealing in technological applications. Moreover, SRO bulk specimens undergo a ferromagnetic transition at $T_C \approx 160$ K, and this makes them applicable in spintronics.[2,3] Band-structure calculations show that the magnetic and transport properties of SRO can be explained by a strong hybridization of oxygen 2*p*-derived states with ruthenium *d* states, which leads to a π^* narrow-type conduction band.[4,5] The magnetic state of SRO is very fragile and depends critically on the overlapping of those orbitals. For instance, as the Ca^{2+} ion is smaller than Sr^{2+}, the perovskite cell of $CaRuO_3$ is more distorted than SRO, and ferromagnetism is suppressed. The metallic state is more robust and compounds, such as $CaRuO_3$ or $BaRuO_3$, still remain metallic,[6] with resistivity values close to that of SRO.

At room temperature, bulk SRO has an orthorhombic structure (Pbnm) with lattice parameters $a = 5.567$ Å, $b = 5.553$ Å, and $c = 7.845$ Å.[7] Because of the small distortions with respect to the ideal cubic perovskite structure, SRO is often indexed in a pseudocubic unit cell with parameter $a_c(\mathrm{SRO}) \approx 3.93$ Å. Thus, the volume of the orthorhombic unit cell is $\approx \sqrt{2}a_c \times \sqrt{2}a_c \times 2a_c$. $SrTiO_3$ (STO) substrate is commonly used for epitaxial growth of SRO. STO has a cubic perovskite structure ($Pm\bar{3}m$) and lattice constant of $a_c(\mathrm{STO}) = 3.905$ Å. If one assumes that when SRO is deposited on a (001) STO substrate, the orthorhombic symmetry of the SRO unit cell is preserved, then the film can grow epitaxially with its (001)°, (110)°, or $(1\bar{1}0)°$ planes parallel to the STO (001) surface (reflections indexed with an orthorhombic unit cell are denoted henceforth by $[h\ k\ l]^0$ Miller indices; those indexed as cubic by $[h\ k\ l]^c$). Therefore, as described by Jiang *et al.*,[8] there are six possible SRO domain structures and orientations: (i) The SRO film can grow with its (110)° plane parallel to the STO $(001)^c$ surface with an in-plane orientation relationship with respect to the STO substrate of either $\mathrm{SRO}[001]° // \mathrm{STO}[010]^c$ and $\mathrm{SRO}[1\bar{1}0]° // \mathrm{STO}[100]^c$ (mode *X*) or $\mathrm{SRO}[001]° // \mathrm{STO}[100]^c$ and $\mathrm{SRO}[1\bar{1}0]° // \mathrm{STO}[010]^c$ (mode *Y*). (ii) The SRO film can also grow with its $(1\bar{1}0)°$ plane parallel to the $(001)^c$ surface of STO with an in-plane orientation relationship of either $\mathrm{SRO}[001]° // \mathrm{STO}[010]^c$ and $\mathrm{SRO}[110]° // \mathrm{STO}[100]^c$ (mode *X′*), or

SRO[001]°//STO[100]^c and SRO[$\bar{1}$10]°//STO[010]^c (mode Y'). (iii) The SRO film grows along its [001]° axis normal to the $(001)^c$ surface of STO, with an in-plane orientation relationship of either SRO[100]°//STO[110]^c and SRO[010]°//STO[1$\bar{1}$0]^c (mode Z), or SRO[100]°//STO[1$\bar{1}$0]^c and SRO[010]°//STO[110]^c (mode Z'). If some of these variants were simultaneously formed during film growth, then multidomain structures would coexist in a thin film.

The presence of multidomains and the concomitant presence of boundaries are expected to affect relevant properties because of the high sensitivity of the magnetotransport properties of SRO to structural disorder. Therefore the growth of twin-free samples exhibiting a single crystallographic orientation would be highly desirable. On the one hand, this would avoid contributions to resistivity arising from twin boundaries. On the other hand, it may allow one to tailor magnetic electrodes with well-defined in-plane components of the magnetic easy axis.[9] Some of these reasons prompted early studies on multidomain formation (and suppression) in SRO films on STO $(001)^c$.

X-ray-diffraction analysis allowed one to determine that SRO films grow with a [110]° texture normal to the substrate and the in-plane texture was investigated by performing φ scans of off-axis nondegenerated peaks.[1,10] It was argued that the domain structure is critically dependent on the STO substrate miscut angle:[10] it was reported that the microstructure of SRO thin films grown on nominally exact STO $(001)^c$ substrates consisted of both X- and Y-type domains with nearly the same volume fraction. In contrast, films grown on large miscut angle substrates ($\theta_V \approx 2°–4°$) were found to be single domain.[10,11]

We note that these statements imply that the unit cell of the SRO films grown on the STO substrate is actually orthorhombic (as it is in bulk SRO at room temperature) and thus strain effects related to epitaxial growth on a cubic substrate (STO) are not explicitly considered. Moreover, the reported x-ray diffraction (XRD) evidences (φ scans) of orthorhombic symmetry of SRO and single domain selection by substrate vicinality are not free of ambiguities.[12] Transmission electron microscopy (TEM)[11] was employed to support the x-ray-diffraction results on the in-plane texture of SRO films grown on STO$(001)^c$ substrates. From these experiments it was concluded that the unit cell is orthorhombic. However, as already signaled by some authors,[13] sample preparation for TEM characterization may promote structural relaxation and thus this conclusion is not free from experimental drawbacks.

In spite of these observations, the use of vicinal STO substrates for the growth of SRO has become the rule, assuming that the absence of multiple cell-orientation variants is at the origin of the observed improved electrical properties.[14]

In this paper we shall revise these issues. We have grown epitaxial SRO films on STO(001) substrates of various vicinalities and thicknesses by pulsed-laser deposition (PLD). By state-of-the-art x-ray-diffraction (XRD) techniques we show that fully strained SRO films are grown on STO $(001)^c$. As a result of the full in-plain strain, the basal unit cell of SRO matches that of the cubic STO substrate, thus imposing a squared in-plane lattice metrics. Below we show that the experimental data indicate that [0 0 1]° SRO axis is in the film plane. Therefore, this implies that $(1/\sqrt{2})d(1\,-1\,0)°$(SRO) [or $(1/\sqrt{2})d(1\,1\,0)°$(SRO)] $=(1/2)d(001)°(\mathrm{SRO}) = a_c(\mathrm{STO}) = 3.905$ Å along the in-plane $[100]^c$ and $[010]^c$ directions of the STO substrate; $d(1\,-1\,0)°$, $d(1\,1\,0)°$ and $d(001)°$ denote the corresponding interplanar distances in SRO. In spite of this coincidence, through extensive use of ψ-φ coupled area scans and μ-Raman spectroscopy, we conclusively show that the in-plane internal symmetry of the unit cell is not square, that is, the [1−10]° (or [1 1 0]°) and the [001]° directions are not equivalent and thus the SRO unit cells are well aligned along a unique direction, forming a single-domain structure (it is in this specific sense that we use the term "twin free"), *irrespective* of the substrate vicinality. Even films grown on STO substrates with a miscut angle as low as $\theta_V \approx 0.1°$ are found to be single domain. That means that even though the films grow perfectly matched to the substrate lattice parameters, there is still some internal degree of freedom, probably defined by rotations of the RuO_6 octahedrons within the unit cell, that defines a nonsquared in-plane internal symmetry. Having established that nonvicinal substrates can be used to obtain twin-free films, we have investigated the role of miscut angle on the magnetotransport properties of films. Interestingly enough, we show that, in close agreement with previous reports, films grown on $\theta_V \approx 2°$ substrates have a far reduced residual resistivity.

From the above two observations we conclude that the enhanced quality of films does not result from an eventual suppression of crystallographic multidomains. Instead, we suggest that it results from a change of growth mode as the substrate miscut angle is modified. Indeed, atomic force microscopy analysis reveals significant morphological changes for vicinalities $\theta_V \approx 2°$. This finding illustrates the relevant role of growth mechanism on functional properties of oxides and emphasizes the importance of substrate nanostructure.

II. EXPERIMENTAL

SRO films were deposited by PLD at a substrate temperature of 750 °C and under 0.1 mbar of pure oxygen. STO(001) substrates with miscut angles within θ_V (0.04°, 0.1°, 0.5°, 1°, 1.5°, 2°, and 4°) were used. We note that $\theta_V \leqslant 0.1°$ corresponds to an almost singular substrate with nominally zero miscut. The miscut angle was determined by x-ray techniques and also from atomic force microscope (AFM) height profiles.

A first set of films were characterized by x-ray-diffraction experiments in a Philips MRD four-circle diffractometer with Cu Kα radiation. A triple-axis configuration was used. As representative examples of the structural differences among samples, we present here data corresponding to the film grown on a singular ($\theta_V \approx 0.1°$) and on a large miscut angle ($\theta_V \approx 1.9°$) STO substrate.

Films with thickness $t \approx 90$ nm were characterized by Raman spectroscopy. Raman spectroscopy experiments were performed using a Jobin-Yvon T64000 confocal μ-Raman spectrometer at room temperature, in a backscattering con-

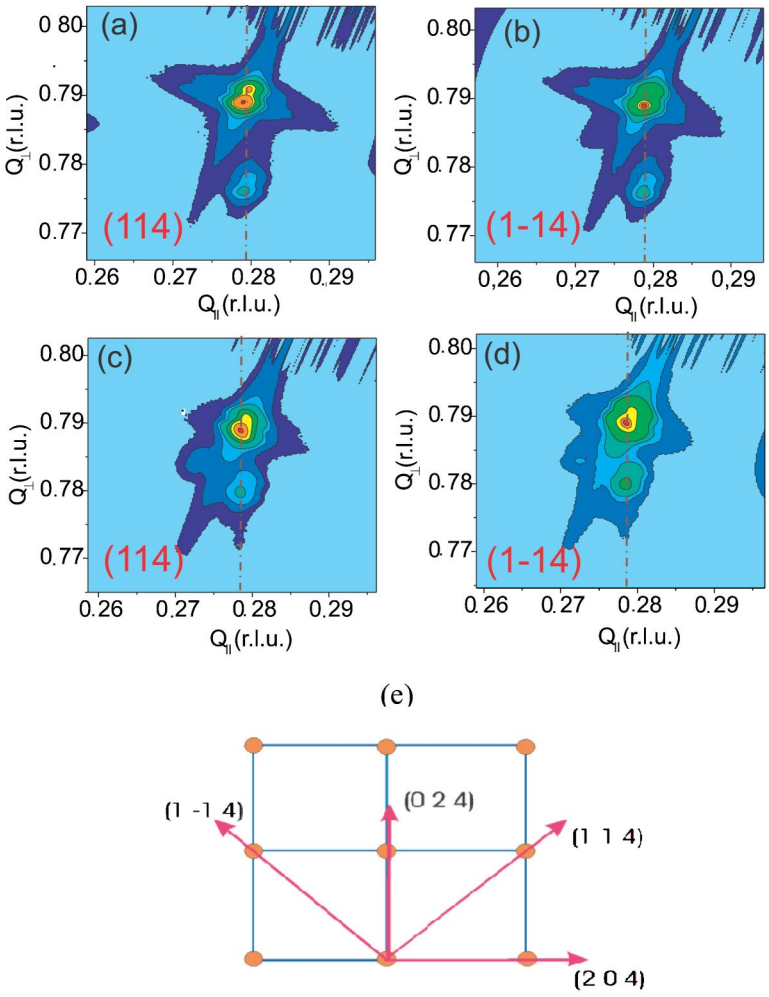

FIG. 1. (Color online) Reciprocal space maps around the (1 1 4) and (1 $\bar{1}$ 4) reflections for SRO films with thickness $t=90$ nm grown on STO (0 0 1) substrates with miscut angle (a,b) $\theta_V \approx 0.1°$ and (c,d) $\theta_V \approx 1.9°$. (e) Schematic illustration of the in-plane scanning directions of reciprocal space maps around (2 0 4), (1 1 4), (0 2 4), and (1 $\bar{1}$ 4) reflections.

figuration. The energy resolution of the spectrometer was set to 1 cm^{-1}, and a Si crystal grown along the [111] direction was used for energy calibration. Measurements were done in a backscattering $z(xx)\bar{z}$ configuration, where z denotes the direction of propagation of light parallel to the growth axis of the sample, and x its polarization.[15] In the $z(xx)\bar{z}$ configuration the polarizer and the analyzer were set parallel to each other. With the aim of probing the in-plane texture, the samples were rotated around the film perpendicular axis. For each rotation angle $\Theta(0° \leqslant \Theta \leqslant 180°)$, a Raman spectrum in the range of energies 140 $cm^{-1} \leqslant \nu \leqslant 500$ cm^{-1} was collected. For these particular experiments and with the aim of being used as reference and comparison, SRO films grown on $LaAlO_3$ (LAO) were also measured. We recall here that SRO films grown on LAO are ubiquitously found to be relaxed with multidomains,[16] owing to the strong twinning of the substrate and the large mismatch.

In order to emphasize the role of substrate and for electrical transport characterization, a series of nanometric films, 3.5 nm and 7 nm thick, have been grown on substrates with miscut (θ_V) angles in the ~0.04°–4° range. Transport measurements were done in a PPMS Quantum Design system with the four-probe method.

A Molecular Imaging atomic force microscope (AFM) in tapping mode was used to explore the film's surface. After appropriate flattening the obtained images were used to determine the miscut angle.

III. RESULTS

A. Domain structure analysis: Reciprocal space maps

We analyze here the domain structure in two characteristic samples, namely, a SRO film grown on a nominally exact STO $(001)^c$ substrate and a SRO film grown on an intentionally miscut 2°-vicinal STO $(001)^c$ substrate. The actual miscut angle values were determined experimentally to be $\theta_V \approx 0.1°$ and $\theta_V \approx 1.9°$, respectively, and the thickness was $t \approx 90$ nm for both films.

Reciprocal space maps (RSM) of both samples were performed around $(204)^c$, $(114)^c$, $(024)^c$, and $(1\bar{1}4)^c$ diffraction peaks. In this way, the eventual presence of in-plane twin behavior could be analyzed, since these RSMs were scanned along different orientations on the in-plane projection of the pseudocubic unit cell [see Fig. 1(e)]. The RSMs for both samples around $(114)^c$ and $(1\bar{1}4)^c$ reflections are displayed in Figs. 1(a) and 1(b) ($\theta_V \approx 0.1°$) and Figs. 1(c) and 1(d) ($\theta_V \approx 1.9°$). Similar results were observed for RSMs measured around $(204)^c$ and $(024)^c$ reflections. We note from Fig. 1(a) that the film and the substrate have a common in-plane pro-

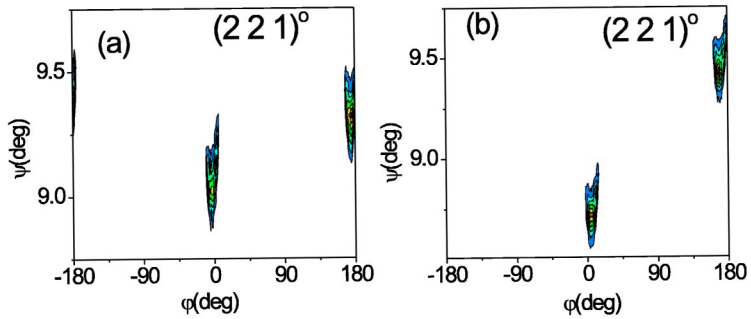

FIG. 2. (Color online) Ψ-ϕ area scans of the $(2\ 2\ 1)^0$ reflection are displayed for a film grown on (a) a nominally exact STO substrate and (b) a STO substrate with $\theta_V \sim 1.9°$.

jection of the reciprocal vector; the same conclusion follows after rotation of 90° [the $(1\bar{1}4)^c$ reflection, Fig. 1(b)]. As a result, the SRO films grow fully strained. As the substrate is cubic it should be concluded that, within the experimental resolution, the pseudocubic unit cell of SRO has a square in-plane metrics, with $(1/\sqrt{2})d(1\ -1\ 0)°(\mathrm{SRO})$ [or $(1/\sqrt{2})\mathrm{d}(1\ 1\ 0)°(\mathrm{SRO})$]$=(1/2)\mathrm{d}(001)°(\mathrm{SRO})=a_c(\mathrm{STO})$ $=3.905$ Å. The same conclusion follows from the observation of the RSMs of the $\theta_V \approx 1.9°$ sample [Figs. 1(c) and 1(d)]. The same behavior was also observed in a SRO film with large thickness $t \approx 320$ nm.[17,18]

A pseudocubic SRO unit cell with equal in-plane lattice parameters is expected from the isotropic strain induced by growth on the cubic STO substrate. However, a square in-plane metrics does not preclude the possibility of having a rectangular in-plane internal symmetry. But RSMs are not the appropriate tool to clarify this issue and, thus, other techniques, such as φ scans of nondegenerated peaks or μ-Raman spectroscopy have been used.

B. Domain structure analysis: φ scans of nondegenerated peaks

Ψ-φ coupled area scans of the nondegenerated (221)° diffraction peaks were performed. We assumed that the SRO films were oriented with the [001]° axis in the film plane. We will show that this assumption is required to satisfactorily explain the results from Raman spectra. The experiments were done on the same two samples described above; that is: $t \approx 90$ nm, $\theta_V \approx 0.1°$ and $\theta_V \approx 1.9°$. The results are displayed in Figs. 2(a) and 2(b). We observe that in both cases, i.e., the films grown on the $\theta_V \approx 0.1°$ [Fig. 2(a)] and on the $\theta_V \approx 1.9°$ [Fig. 2(b)] STO substrates, the Ψ-φ coupled area scans show *only* two peaks separated by $\Delta\varphi \approx 180°$ of each other. This means that although the in-plane metrics is square, the internal symmetry of the unit cell is not. Moreover, these observations indicate that both films display a single-domain orientation. The presence of orthogonal domains should be manifested by the presence of two sets of peaks, split 180°, and dephased by 90°. Certainly this is not observed in Fig. 2. It thus follows that not only are the films grown on vicinal substrates twin-free, as expected, but also the film grown on the nominally exact $(\theta_V \approx 0.1°)$ substrate has a single crystallographic domain. This is a quite striking result because, as mentioned above, as a rule of thumb large miscut substrates are often used to obtain single-domain SRO films.[1,9,10,19]

The main result presented here, namely, the single orientation of the orthorhombic unit cell even for films grown on nominally exact substrates, is confirmed by μ-Raman spectroscopy, as described in Sec. III C.

C. Domain structure analysis: μ-Raman spectroscopy

Two SRO films, one grown on a STO(001) substrate and the other on LAO (001) substrate have been characterized by μ-Raman spectroscopy. In both cases, the substrates were nominally exact, with an actual miscut angle of $\theta_V \approx 0.1°$, and their thickness was $t \approx 160$ nm. Spectra were collected in backscattering configuration along the growth direction of the films, with the polarizer and analyzer set parallel to each other. A series of spectra were obtained rotating the films an angle Θ around their normal axis. The results collected for $\Theta = 0°$ and 90° are displayed (top and bottom) for both films in Figs. 3(a) and 3(b) for SRO films on STO and LAO, respectively. The low-energy modes around 200–240 cm^{-1} have an intensity that is almost independent on Θ; this is consistent with a A_g symmetry of this mode as reported by Iliev *et al.*[20] On the other hand, inspection of data in Fig. 3(a) clearly reveals features in the spectra of SRO on STO, particularly noticeable in the region around 350–410 cm^{-1}, that largely evolves with Θ. On the contrary, the 350–410 cm^{-1} modes of SRO films on LAO [Fig. 3(b)] do not display a significant variation with Θ. These variations in the spectra reflect both the symmetry of the corresponding phonon modes and the symmetry of the film. From the comparison of the spectra taken at 0° and 90° (top and bottom) for SRO on STO and LAO films [Figs. 3(a) and 3(b)] it follows that there is a clear evolution of the 350–410 cm^{-1} modes for SRO grown on STO, whereas the relative intensity of the corresponding modes of SRO films on LAO remains almost unchanged.

Three phonon modes were identified in the region around 350–410 cm^{-1}: two modes of B_{1g} symmetry (353 and 398 cm^{-1}) and one mode of A_g symmetry (373 cm^{-1}).[20] Notice that there is a shift to higher energies of up to 3 cm^{-1} in the position of the phonon modes when comparing both samples, indicating that the SRO film grown on STO is under in-plane compressive strain, in agreement with the x-ray analysis of the films performed in Sec. III A.

To simplify the discussion, we will refer to the analysis performed on the phonon mode at 373 cm^{-1} to determine the crystallographic orientation of the samples and will focus our attention on the mode at 398 cm^{-1} to study the domain struc-

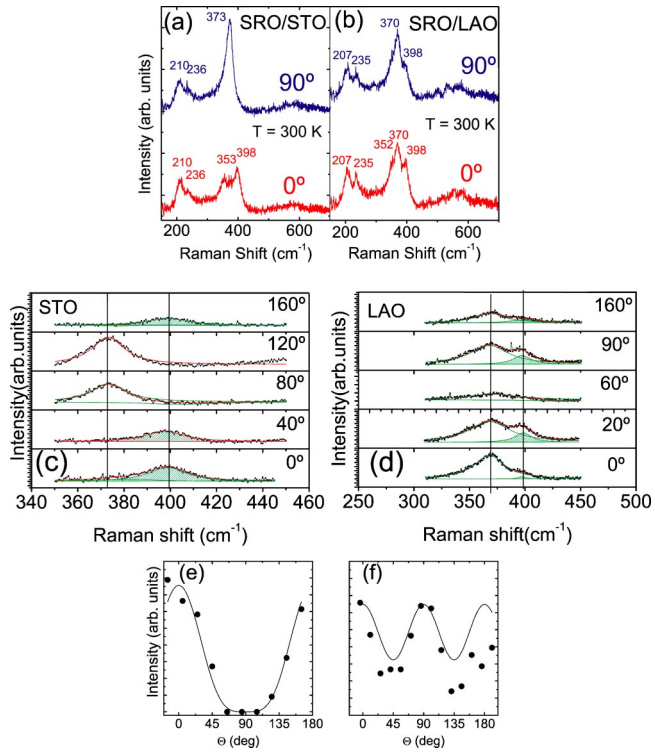

FIG. 3. (Color online) Raman spectra recorded at angles $\Theta = 0°$, 90° for films grown on nominally exact (a) STO and (b) LAO substrates. The intensity of the Raman peaks at ~398 cm^{-1} as a function of Θ, for SRO films grown on (c) STO and on (d) LAO were evaluated by fitting the spectra using Lorentzian lines. The area under the fitted curves is shadowed. The Θ dependence of the peak intensity of the phonon mode at ~398 cm^{-1} measured in a $z(xx)\bar{z}$ configuration is displayed in (e) for the film on STO and in (f) for the film on LAO. The continuous line in (e) corresponds to Eq. (4). For (f), we have considered Eq. (4) and its orthogonal rotation representing domains that occupy the same scattering volume.

ture of the films. Figures 3(c) and 3(d) show the Raman spectra around the 373 cm^{-1} and 398 cm^{-1} modes as a function of the angle Θ. In order to extract information from the measured spectra, Raman peaks were deconvoluted by fitting the spectral profiles with Lorentzian curves and the corresponding areas were determined. A linear background below each Raman peak was determined by extrapolation and subtracted from the spectrum before peak fitting. The evolution of the intensity of the 398 cm^{-1} mode as a function of Θ is visualized by the shadowed areas comprised under the fitted curves in Figs. 3(c) and 3(d). From this picture, a clear-cut different behavior between both films is observed. This is more easily observed when the angular dependence of the measured extracted intensity is plotted for the whole range of measured Θ values. In Figs. 3(e) and 3(f) we collect the angular dependence of the intensity of the ~398 cm^{-1} mode for the SRO film on STO and LAO, respectively. Inspection of data in Fig. 3(e) reveals that the measured intensity for the SRO on STO film has a period of about 180°, whereas in the case of SRO on LAO [Fig. 3(d)] the intensity appears to display an intermediate behavior, with a period of 90°. In order to analyze, in detail, these data, the symmetry of the corresponding phonon modes shall be considered. For this purpose we have used the orthorhombic space group of bulk SRO (Pbnm). The corresponding Raman tensors for phonon modes of A_g and B_{1g} symmetry are given by

$$A_g \leftrightarrow \begin{pmatrix} \alpha & 0 & 0 \\ 0 & \beta & 0 \\ 0 & 0 & \gamma \end{pmatrix}, \tag{1a}$$

$$B_{1g} \leftrightarrow \begin{pmatrix} 0 & \varepsilon & 0 \\ \varepsilon & 0 & 0 \\ 0 & 0 & 0 \end{pmatrix} \tag{1b}$$

where α, β, and γ stand for the A_g tensor components along the x, y, and z directions, and ε is the B_{1g} tensor component corresponding to the x-y directions. According to the results of Iliev *et al.*,[20] the A_g mode at 373 cm^{-1} is characterized by a large value of the polarizability along the [001]° axis, with $\gamma \gg \alpha \approx \beta$. Based on this fact and making use of the tensors given by Eqs. (1a) and (1b), we can calculate the angular dependence of the peak intensity, which depends on the orientation of the domains in the crystal and on the polarization of the incident and scattered light. If the growth axis were along the [001]° direction, the intensity of the A_g-phonon modes would follow the expression

$$\left[\frac{\alpha}{2}\cos^2\Theta + \frac{\beta}{2}\sin^2\Theta\right]^2 \tag{2}$$

Taking into account that $\alpha \approx \beta$, this equation would predict no change in intensity of the A_g modes with Θ, a result which is in obvious disagreement with the angular evolution of the A_g phonon mode at 373 cm^{-1} of SRO//STO [see Fig. 3(c)]. Thus, the angular evolution of this mode indicates that the [001]° axis of SRO//STO lies in the film-plane. As a consequence, the intensity of the A_g-phonon modes follows the expression

$$\left[\left(\frac{\alpha}{2} + \frac{\beta}{2}\right)\cos^2\Theta + \gamma\sin^2\Theta\right]^2, \tag{3}$$

whereas for a Raman phonon of B_{1g} symmetry it is given by

$$\left[\frac{\varepsilon}{2}\cos^2\Theta\right]^2. \tag{4}$$

We note that Eq. (3) predicts that the intensity of phonons with A_g symmetry, as a function of Θ, will remain constant for those modes for which $\alpha = \beta = \gamma$. This is the case of the modes around 200–240 cm^{-1}. In contrast, for the mode with $\gamma \gg \alpha = \beta$ at 373 cm^{-1} a signal with a period of 180° is expected, with a maximum amplitude for $\Theta = 90°$. Equations (3) and (4) reproduce the angular evolution of the peaks of the SRO/STO sample provided that $\Theta = 90°$ corresponds to a direction of polarization parallel to the [001]°. From the previous discussion we conclude that: (i) in spite of the fact that the length of the in-plane lattice parameters of the SRO/STO sample are proved to be equal by x-ray analysis, the in-plane unit cell has an orthorhombic symmetry, evidenced by the fact that the A_g mode at 373 cm^{-1} shows much larger intensity for polarization along the [001]° axis than perpendicular

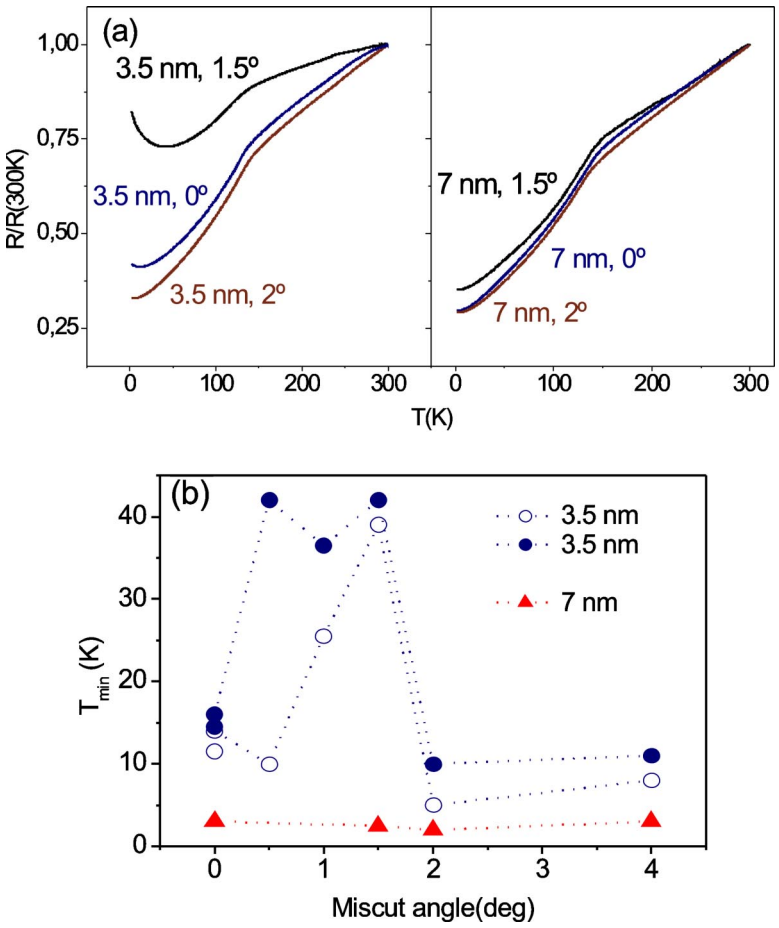

FIG. 4. (Color online) (a) The temperature dependence of the resistance is plotted for films grown on STO (0 0 1) substrates with miscut angle $\theta_V = 0.04°, 1.5°$, and $\theta_V = 4°$ with thickness $t = 3.5$ nm (left panel) and $t = 7$ nm (right panel). The resistance has been normalized to the value at 300 K. (b) The temperatures T_{min} at which the minima of $R(T)$ appear are plotted against the substrate miscut angle.

to it; (ii) the film grown on LAO has a two-domain structure with the orthorhombic unit cell oriented at 90° of each other, as expected from the twinning of the LAO substrate. This observation explains why the peak intensity of the 398 cm^{-1} phonon mode [Fig. 3(f)] has a period of 90°, instead of the 180° period observed for the twin-free film grown on STO.

The results of the analysis of Raman spectra are in agreement with those of φ scans of nondegenerated diffraction peaks explained in the last section, i.e., the unit cell of SRO films grown on STO substrates has an orthorhombic symmetry although its metrics is tetragonal, and the films show a single crystallographic domain. In contrast, the angular dependence of the peak intensity of the same phonon mode measured in the film grown on LAO can be explained by assuming a multidomain structure. It is worth stressing that the internal in-plane asymmetry of the unit cell, related to the buckling of the oxygen octahedrons, is preserved in these fully strained films, although the metrics of the unit cell is forced to be tetragonal because of the clamping to the substrate. Our results on SRO on STO are along the same lines of recent reports[21] on the cubic-to-tetragonal phase transition occurring in $SrTiO_3$ at about 105 K, which, in substrate-induced strained films, still occurs but without any change of the shape of the unit cell lattice. These observations illustrate the relevance of substrate-induced clamping effects on phase transitions and domain formation in epitaxial films.

IV. TRANSPORT PROPERTIES OF ULTRATHIN SRO FILMS

The effect of the growth-induced disorder on the transport properties was investigated in epitaxial SRO ultrathin films ($t = 3.5$ nm, 7 nm) grown on as-received STO(0 0 1) substrates with different miscut angles ($0.04° \leqslant \theta_V \leqslant 4°$). Figure 4(a) shows the measured resistance values, normalized to the values at high temperature, for films grown on 0.04°, 1.5°, and 4° substrates for films with thickness $t = 3.5$ nm (left panel) and $t = 7$ nm (right panel). Inspection of data in Fig. 4(a) reveals the presence of resistivity minima at low temperature. This phenomenon is closely related to the amount of structural disorder. Stronger disorder is revealed by a higher value of T_{min}, i.e., the temperature at which the resistivity minima appear. Thus, the evolution of T_{min} with the substrate miscut angle reflects the evolution of growth-induced disorder.[18] It is found that the values of T_{min} are strongly dependent on the substrate miscut angle, as emphasized in Fig. 4(b). The resistance was measured by injecting current along two orthogonal in-plane directions. The experimental data revealed the presence of an in-plane anisotropic resistance that was more prominent in the thinner series of films, related to the anisotropic growth mode occurring at early stages of growth.[22] For that reason, Fig. 4(b) shows two different T_{min} values for $t = 3.5$ nm series because of the resistance anisotropy, but only one value for the $t = 7$ nm, where this anisotropy virtually vanished.

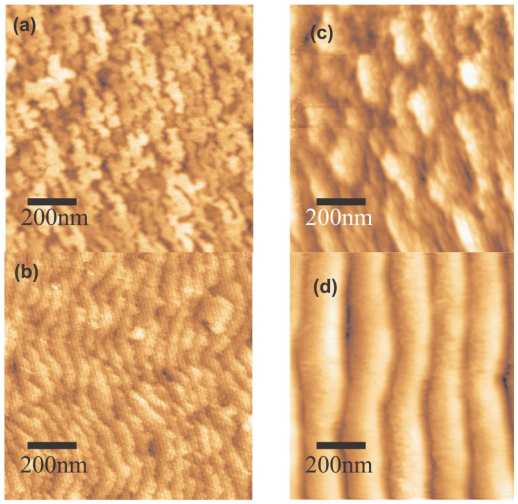

FIG. 5. (Color online) AFM topographic images corresponding to films grown on $\theta_V=0.5°$ substrates with thickness (a) 1.75 nm and (b) 14 nm and to films grown on $\theta_V=2°$ substrates with thickness (c) 1.75 nm and (d) 100 nm.

From Figs. 4(a) and 4(b) it is clear that the transport properties are strongly dependent on the film thickness and the substrate miscut angle. We observe first that films with thickness $t=7$ nm show low T_{min} values (below 5 K), indicating that the growth-induced structural disorder is significantly lower than in films with thickness $t=3.5$ nm. This can be understood by assuming that disorder develops in the regions near the interface, and its effects become less significant when the film thickness is larger. On the other hand, within the series of thickness $t=3.5$ nm, the T_{min} values are particularly high ($T_{min}\sim 30$–40 K) for films grown on substrates with $\theta_V=0.5$–$1.5°$. For films grown on substrates with $\theta_V \approx 2°$, the growth-induced structural disorder is significantly reduced.

In order to understand the previous results, we have analyzed the data from surface morphologies of SRO films obtained from AFM measurements. Figures 5(a) and 5(b) show the AFM images of films grown on 0.5° STO substrates with thickness $t\approx 1.75$ nm (a) and $t\approx 14$ nm (b). In these conditions, it was observed that at the early stages there is a fingerlike structure originated by three-dimensional islands that nucleated along the substrate steps.[22] Afterward, adatoms stick preferentially in the valleys of the structure and the films become progressively smoother. Above a certain thickness, the films are extremely flat and have a structure of terraces and steps, with the growth proceeding by a step flow or by a layer-by-layer mechanism, depending on the exact value of the substrate miscut angle.[23] Highly disordered zones are expected to form at the boundaries where the coalescence of the fingers occurs. Since steps are closer as the miscut angle increases, the number of formed fingers increases and the growth-induced disorder is expected to be larger. This might explain the larger disorder in film grown on the 0.5° substrate than the one grown on the 0.1° substrates [see Fig. 4(b)].

In contrast, the surface morphologies of films grown on 2° STO substrates with thickness $t\approx 1.75$ nm [Fig. 5(c)] and $t \approx 100$ nm [Fig. 5(d)] reveal that film growth is clearcut different. We observe in Fig. 5(c) a lobulelike structure with a typical size of about 200 nm. Inspection of Fig. 5(d) indicates that this structure evolves into a formation of bunched steps, with a typical separation between steps of about 200 nm. Especially significant is the comparison of Figs. 5(a) (0.5° substrate) and 5(c) (2° substrate). For the former, the nearly coalescing fingerlike units have a typical width of about 50 nm, whereas for the latter, the nearly coalescing lobulelike units have a typical size of about 200 nm. It is expected, then, that the growth-induced disordered regions, mostly located at regions where coalescence occurs, should be more significant for the film grown on the 0.5° substrate. This might explain why the electrical properties of the film grown on the 2° substrates are improved [see Fig. 4(b)].

These remarks indicate that the electrical properties of SRO films are not solely determined by the crystallographic structure. As pointed out above, it has been argued that SRO films must be grown on vicinal STO substrates with large enough miscut angles in order to have a single-domain orientation of the orthorhombic unit cell and avoid twin boundaries. This has been established as a necessary premise to have high-quality SRO films. However, we have demonstrated that our films are twin-free even when grown on 0.1° substrates. In spite of this, we observe that the transport properties of epitaxial SRO ultrathin films are strongly dependent on the miscut angle. Bearing in mind the strong dependence of the growth mode on the substrate miscut angle, it is reasonable to ascribe the change of the transport properties to the change of the growth mode. The anisotropic growth mode along substrate steps at early stages induces a structural disorder that is localized at the regions where the finger-like units coalesce. Within this picture, one can reasonably argue that the growth-induced disorder will be strongly dependent on those parameters that, as the substrate miscut angle, determine the growth mode. These findings emphasize that not only the film epitaxy and texture must be carefully analyzed, but that careful attention must be paid to those parameters having an impact on the film growth and inducing disorder at local level, which might be hardly detected by conventional experimental tools, such as x-ray diffraction.

V. SUMMARY

In this paper we have first shown that SRO films grow fully strained on STO substrates and have an in-plane squared lattice. However, the internal degree of freedom, likely determined by rotations of the RuO_6 octahedrons, still induces the existence of a well-defined in-plane anisotropic axis (reminiscent of the orthorhombic symmetry of bulk). That means that the oxygen octahedrons rotate as expected to occur across the cubic to orthorhombic high-temperature phase transition, although the in-plane lattice parameters of the pseudocubic SRO unit cell are clamped to that of the substrate. Under the used growth conditions and the well-matched STO substrate, a single orientation of this in-plane anisotropy axis exists and thus SRO films on STO are twin-free. We have demonstrated that our films are single domain

even when grown on STO substrates with $\theta_V \approx 0.1°$; thus, large vicinalities of substrates are not a prerequisite to obtain single-domain SRO films.

The transport properties of SRO ultrathin films are found to be strongly dependent on thickness and on the substrate miscut angle. In particular, it is seen (in agreement with previous reports) that films grown on large miscut angle substrates show lower residual resistivities and higher residual resistance ratios. As all films are twin-free, we conclude that the striking change of the magnetotransport properties with the miscut angle cannot be attributed to an untwining of the orthorhombic unit cell for films grown on large miscut substrates, but originates from a change of the growth mode and the resulting microstructure. These findings are relevant in several contexts. First, they show that phase transition and twin formation in epitaxial films can take place differently from in bulk, as they may occur without changes in unit cell volumes or shape. Second, they illustrate the critical role of the mechanism of film growth and epitaxial formation on functional properties of oxides.

ACKNOWLEDGMENTS

Financial support by the CICYT of the Spanish Government (Projects No. MAT2002-04551-C03 and No. MAT2003-4161) and a TMR Grant from the European Union, HPRN-CT2000-00021 are acknowledged.

[1] C. B. Eom, R. J. Cava, R. M. Fleming, J. M. Philips, R. B. van Dover, J. H. Marshall, J. W. P. Hsu, J. J. Krajewski, and W. F. Peck, Science **258**, 1766 (1992).

[2] G. Herranz, B. Martínez, J. Fontcuberta, F. Sánchez, M. V. García-Cuenca, C. Ferrater, and M. Varela, J. Appl. Phys. **93**, 8035 (2003).

[3] K. S. Takahashi, A. Sawa, Y. Ishii, H. Akoh, M. Kawasaki, and Y. Tokura, Phys. Rev. B **67**, 094413 (2003).

[4] I. I. Mazin and D. J. Singh, Phys. Rev. B **56**, 2556 (1997).

[5] P. B. Allen, H. Berger, O. Chauvet, L. Forro, T. Jarlborg, A. Junod, B. Revaz, and G. Santi, Phys. Rev. B **53**, 4393 (1996).

[6] M. Shepard, S. McCall, G. Cao, and J. E. Crow, J. Appl. Phys. **81**, 4978 (1997)

[7] C. W. Jones, P. D. Battle, P. Lightfoot, and W. T. A. Harrison, Acta Crystallogr., Sect. C: Cryst. Struct. Commun. **45**, 365 (1989).

[8] J. C. Jiang, W. Tian, and X. Q. Pan, Q. Gan, and C. B. Eom, Appl. Phys. Lett. **72**, 2963 (1998).

[9] L. Klein, J. S. Dodge, C. H. Ahn, J. W. Reiner, L. Mieville, T. H. Geballe, M. R. Beasley, and A. Kapitulnik, J. Phys.: Condens. Matter **8**, 10111 (1996).

[10] Q. Gan, R. A. Rao, and C. B. Eom, Appl. Phys. Lett. **70**, 1962 (1997).

[11] A. F. Marshall, L. Klein, J. S. Dodge, C. H. Ahn, J. W. Reiner, L. Mieville, L. Antagonazza, A. Kapitulnik, T. H. Geballe, and M. R. Beasley, J. Appl. Phys. **85**, 4131 (1999).

[12] The peak intensities measured with φ scans are strongly affected by the sample misalignment on the goniometer of the diffractometer.

[13] Some authors point to the possibility that orthorhombic domains could appear because of a strain-relaxation phenomenon occurring during TEM specimen preparation.See, for instance, Sang Ho Oh and Chan-Gyung Park, J. Korean Phys. Soc. **37**, 961 (2000), or X. Q. Pan, J. C. Jiang, and W. Tian, Q. Gan, R. A. Rao, and C. B. Eom, J. Appl. Phys. **86**, 4188 (1999).

[14] L. Klein, Y. Kats, A. F. Marshall, J. W. Reiner, T. H. Geballe, M. R. Beasley, and A. Kapitulnik, Phys. Rev. Lett. **84**, 6090 (2000).

[15] D. L. Rousseau, R. P. Bauman, S. P. S. Porto, J. Raman Spectrosc. **10**, 253 (1981).

[16] D. B. Kacedon, R. A. Rao, and C. B. Eom, Appl. Phys. Lett. **71**, 1724 (1997)

[17] F. Sánchez, M. V. García-Cuenca, C. Ferrater, M. Varela, G. Herranz, B. Martínez, and J. Fontcuberta, Appl. Phys. Lett. **83**, 902 (2003).

[18] G. Herranz, B. Martínez, J. Fontcuberta, F. Sánchez, C. Ferrater, M. V. García Cuenca, and M. Varela, Phys. Rev. B **67**, 174423 (2003).

[19] J.-P. Maria, H. L. McKinstry, and S. Trolier-McKinstry, Appl. Phys. Lett. **76**, 3382 (2000).

[20] M. N. Iliev, A. P. Litvinchuk, H. -G. Lee, C. L. Chen, M. L. Dezaneti, C. W. Chu, V. G. Ivanov, M. V. Abrashev, and V. N. Popov, Phys. Rev. B **59**, 364 (1999).

[21] F. He, B. O. Wells, Z.-G. Ban, S. P. Alpay, S. Grenier, S. M. Shapiro, W. Si, A. Clark and X. X. Xi, Phys. Rev. B **70**, 235405 (2004).

[22] G. Herranz, B. Martínez, J. Fontcuberta, F. Sánchez, M. V. García-Cuenca, C. Ferrater, and M. Varela, Appl. Phys. Lett. **82**, 85 (2003).

[23] F. Sánchez, G. Herranz, I. C. Infante, J. Fontcuberta, M. V. García-Cuenca, C. Ferrater, and M. Varela, Appl. Phys. Lett. **85**, 1981 (2004).